2023

High-Sensitivity Vector Bend Sensor Based on a Fiber Directional Coupler Inscribed by a Femtosecond Laser

Ke Tian

Mingyuan Zhang

Chuanzhein Zhao

See next page for additional authors

Funder: National Natural Science Foundation of China (NSFC) (62225502, 61935006, 62090062, 62205085); Heilongjiang Provincial Natural Science Foundation of China (LH2020F028); Fundamental Research Funds for the Central Universities (3072022TS2504); 111 Project (B13015); Heilongjiang Touyan Innovation Team Program; Science Foundation Ireland under the Centres research program for the MaREI project (SFI/12/RC/2302_P2)

Authors

Ke Tian, Mingyuan Zhang, Chuanzhein Zhao, Huibin Li, Shilong Li, Yuxuan Jiang, Gerald Farrell, and Pengfei Wang

High-sensitivity vector bend sensor based on a fiber directional coupler inscribed by a femtosecond laser

KE TIAN,[1,5] MINGYUAN ZHANG,[1] CHUANZHEN ZHAO,[1] HUIBIN LI,[1] SHILONG LI,[2] YUXUAN JIANG,[1] ELFED LEWIS,[3] GERALD FARRELL,[4] AND PENGFEI WANG[1,6]

[1]*Key Laboratory of In-fiber Integrated Optics of Ministry of Education, College of Physics and Optoelectronic Engineering, Harbin Engineering University, Harbin 150001, China*

[2]*Okinawa Institute of Science and Technology Graduate University, Onna, Okinawa 904-0495, Japan*

[3]*Optical Fibre Sensors Research Centre, Department of Electronic and Computer Engineering, University of Limerick, Limerick, Ireland*

[4] *Photonics Research Center, Technological University Dublin, Grangegorman Campus, Dublin 7, Ireland*

[5]*e-mail: ketian@hrbeu.edu.cn*

[6]*e-mail: pengfei.wang@tudublin.ie*

Received XX Month XXXX; revised XX Month, XXXX; accepted XX Month XXXX; posted XX Month XXXX (Doc. ID XXXXX); published XX Month XXXX

In this letter, we demonstrate a high sensitivity vector bend sensor based on a fiber directional coupler. The fiber directional coupler is composed of two parallel waveguides inscribed within a no-core fiber (NCF) by a femtosecond laser. Since the two written waveguides have closely matched refractive indices and geometries, the transmission spectrum of the fiber directional coupler possesses periodic resonant dips. Such a fiber directional coupler exhibits good bending-dependent spectral shift response due to its asymmetric structure. Experimental results show that bending sensitivities of -97.11 nm/m^{-1} and 58.22 nm/m^{-1} are achieved for the 0° and 180° orientation in the curvature range of 0-0.62 m^{-1}, respectively. In addition, the proposed fiber directional coupler is shown to be insensitive to external humidity changes, thus improving its suitability in high-accuracy bending measurements. © 2023 Optical Society of America

http://dx.doi.org/10.1364/OL.99.099999

The measurement and monitoring of bending is often a necessity in areas such as structural health monitoring, biomorphic robotics, and computer vision [1, 2]. Various styles of fiber–based vector bending sensors have been developed based on different fiber configurations, such as fiber gratings [3, 4], Mach-Zehnder interferometers (MZIs) [5-7], a Michelson interferometer [8], a multimode interference device [9], and a photonic crystal fiber (PCF) based interferometer [10]. All the bending sensors mentioned above can achieve bending discrimination in multiple directions, but with the limitation that their bending measurement sensitivities are generally limited to a range of 0.28-45.8 nm/m^{-1}.

Fiber directional couplers has been demonstrated to be sensitive to bending, with a non-vector measurement sensitivity up to -137.87 nm/m^{-1} [11]. Fiber directional couplers have been successfully constructed through two-core fiber [11, 12] and PCF [13]. However, fiber directional couplers constructed with special fibers are limited by their fixed geometry and lack the design freedom available with spatially asymmetric structures and this in turn hinders their application in vector bending measurement. In contrast, femtosecond laser (fs) written fiber directional coupler provide flexible waveguide design freedom [14]. For instance, a hybrid cladding waveguide coupler has been written in a single-mode fiber (SMF) using a fs laser for vector bending measurement [15]. However, due to the weak evanescent field of the fixed-size SMF core, the bending measurement sensitivity, which has a value of 14.8 nm/m^{-1}, for this structure is relatively low.

In this letter, a high sensitivity vector bend sensor is described in which the fiber directional coupler utilizes two parallel waveguides written in a no-core fiber (NCF) using a fs laser. Compared to the common couplers constructed in SMFs, the two waveguides written in the NCF have more closely matched RIs and geometries, resulting in periodic resonant dips. The fiber directional coupler exhibits a good bending-dependent spectral shift response, and a maximum bending sensitivity of -97.11 nm/m^{-1} is achieved. The fiber directional coupler is schematically illustrated in Fig. 1(a), where a section of no-core fiber (NCF) with a length L_1 is spliced between two SMFs (Corning, SMF-28). One straight waveguide (WG_1) is written along the center axis of the NCF, which connects the cores of the two SMFs. To enhance the input and output coupling efficiency for WG_1, the two ends of WG_1 are embedded into the cores of the input/output SMFs, with a length L_3 in both cases [16]. Another straight waveguide (WG_2) is inscribed parallel to WG_1 with a length of L_2 to form the complete fiber directional coupler. The written width of the two waveguides is D and the spacing between the two waveguides centers is X.

According to the mathematical formulation for modeling the mutual light-wave interactions between two parallel optical waveguides, the coupling coefficient κ can be calculated from the following expression

$$\kappa = \frac{\sqrt{2\Delta}}{a}\frac{U^2}{V^3}\frac{K_0\left(\frac{Ws}{a}\right)}{K_1^2(W)} \quad (1)$$

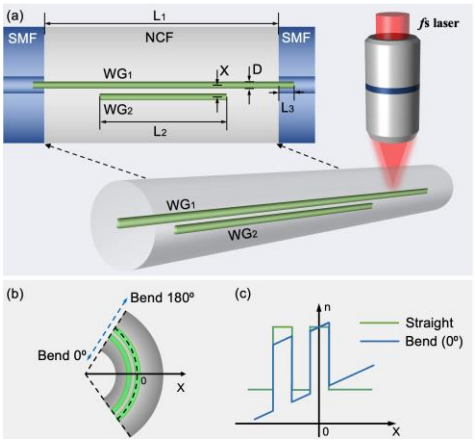

Fig. 1. Schematic diagram of (a) the fs laser written fiber directional coupler; (b) the coupler bending at 0° and 180°; (c) the RI distribution at the straight and 0° bending directions.

where a is the radius of the two waveguides, s is the center separation distance between them, and Δ is the relative RI difference which is determined by $\Delta=(n_1^2-n_2^2)/n_1^2$, where n_1 and n_2 are the RIs of the written waveguides and the NCF. K_0 and K_1 are the modified Hankel functions of order 0 and 1, respectively. V is the normalized frequency, and U and W are the normalized transverse propagation constants of the LP_{01} mode in the core and cladding, respectively. The transmission power P of the directional coupler can be expressed as [17]:

$$P(\lambda) = P_0 \cos^2(\kappa L_0) \quad \textbf{(2)}$$

where P_0 is the initial power and L_0 is the effective coupling length.

As a result of the stress-optical effect, when the fiber structure is bent, the internal stress will cause a change in the RI of the fiber. Specifically in Fig. 1(b), we define the bending angles of 0° and 180° of the fiber directional coupler. Fig. 1(c) presents the corresponding RI profile of the fiber directional coupler at 0° orientations. The RI distribution of the fiber bent towards the x direction can be expressed approximatively by [18]

$$n'(x) = n_0(1 + x \cdot C) \quad \textbf{(3)}$$

where n_0 and C are the RI distribution and the curvature of the directional coupler, respectively. Due to the different positions of the two waveguides in the NCF, the RI difference between them varies with the bending of the coupler. The change of the RI difference of the two parallel waveguides will affect the coupling coefficient κ, combined with the change of the effective coupling length L_0, resulting the shift of the resonance wavelength.

A flow diagram for the fiber directional coupler fabrication is shown in Fig. 2. Firstly, a 1 cm length NCF was spliced between two SMFs to form a singlemode-no core-singlemode (SNS) fiber structure. In this case, multimode interference (MMI) occurs in the NCF section, resulting in spectral dips in Fig. 2(a). Then, a fs laser (Solstice Ace) with a central wavelength of 800 nm, a pulse duration of 100 fs, and a repetition rate of 1 kHz was used to inscribe the waveguides. The laser beam was focused on the center of the fiber through a microscope objective (40X, NA 0.64, Olympus). The SNS fiber structure was mounted on a precision 3-D platform (Newport Corp.) which allowed precise computer-controlled motion during the inscription process. In the writing

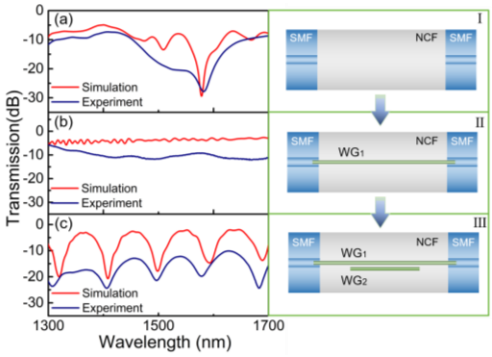

Fig. 2. Transmission spectra and schematic diagrams of (a) an SNS fiber structure with 1 cm length NCF; (b) WG_1 writing in the SNS; (c) Complete WG_1 and WG_2 writing in SNS fiber structure.

process, the laser pulse energy was adjusted to approximately 1.5 μJ and the translational velocity of the fiber was set to 20 μm/s. During the fabrication processes, the fiber directional coupler was connected to a supercontinuum source (SC, YSL) and an optical spectrum analyzer (OSA, YOKOGAWA AQ6370D) to monitor the transmission spectrum in real-time. Based on the selection of waveguide parameters described in [16] combined with real-time monitoring using the OSA, a WG_1 with a width D of 3 μm connecting the SMFs at both ends was fabricated, with the depth L_3 set to approximately 50 μm.

After the first waveguide was inscribed, the output spectrum was tested as shown in Fig. 2(b). It can be seen that the MMI was significantly weakened, which proved that the inscribed WG_1 is effectively coupling the light from the input SMF to the output SMF, suppressing MMI in the NCF as a result. The fs laser parameters used to inscribe WG_2 are the same as those used for WG_1. To obtain a high spectral extinction ratio (ER) while having well-defined resonance dips, a series of simulations were undertaken, from which it was found that the best choices for the length L_2 of WG_2 and the distance between the centers of the two waveguides X were determined to be 8000 μm and 6 μm. As shown in Fig. 2(c), there is an obvious coupling between the fabricated two waveguides, and a series of resonant dips were produced. The measured dip positions are consistent with the simulated spectrum and the maximum ER of the fiber directional coupler is up to 9.8 dB. Due to the diameter mismatch between the WG_1 and SMF core, the insertion loss of the fiber directional coupler is about -12 dB.

The microscope image of the fabricated waveguides is shown in Fig. 3(a), with clear evidence of the two waveguides written in parallel to the center of the NCF. Fig. 3(b) is the cross-sectional image of the fiber directional coupler, and Fig. 3(c) is an enlarged view. The written position of the waveguides can be clearly seen in these two microscope images, where the profiles of the two waveguides are approximately rectangular. The waveguide width D and the waveguide depth h from the NCF center for WG_1 and WG_2 are 3 μm and 12 μm, respectively, and the center distance X between the two waveguides is 6 μm. The RI distribution of the fiber directional coupler was measured by a RI analyzer (Photon Kinetics, S14) with line scanning. The schematic for the scan direction is illustrated in Fig. 3(d), and the corresponding result is shown in Fig. 3(e). It is clear that a positive RI modulation is induced at the waveguide position, and the average RI difference between the waveguides and NCF is about 0.005.

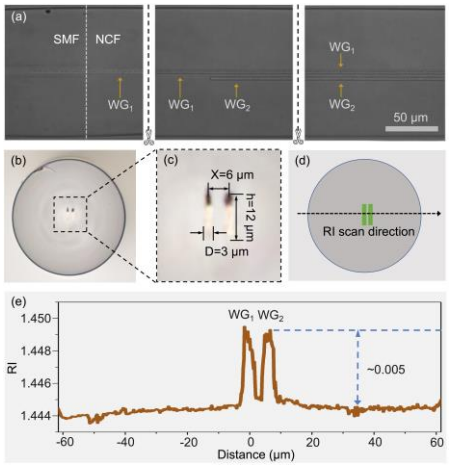

Fig. 3. (a) Microscope images of the fiber directional coupler. (b) Cross-sectional image. (c) Enlarged image of the waveguide section. (d) Schematic of the RI scan direction using line scanning. (e) Measured RI distribution.

The transmission optical field distribution within the fiber directional coupler was simulated based on the Beam Propagation Method (BPM). In the simulation, the entire waveguide region was assigned a positive RI modulation, while the weak negative RI modulation was ignored. The simulation parameters used were: the core/cladding diameters and RI for the SMF are 8.3/125 μm and 1.4504/1.4447, the diameter of the NCF is 125 μm and its RI is 1.444, the inscribed waveguides have a RI of 1.449, with the following dimensional parameters: D=3 μm, h=12 μm, X=6 μm, L_1=10000 μm, L_2=8000 μm, L_3=50 μm. As shown in Fig. 4(a), light can be efficiently transmitted from the SMF core into the WG_1 and coupled between the two inscribed waveguides. Fig. 4(b) presents simulated mode field distribution results at wavelengths of 1525 nm and 1550 nm, respectively. It can be observed that most of the light energy is distributed in WG_1 at 1525 nm, while when the incident light wavelength is tuned to 1550 nm, most of the light energy shifts is coupled to WG_2. This light coupling phenomenon was also demonstrated by experiments. The mode profile of WG_1 and WG_2 was tested using a tunable laser light source (Santec, TSL-710) and a CCD camera (Newport, LBP2-HR-IR), and the measured results are shown in Fig. 4(c).

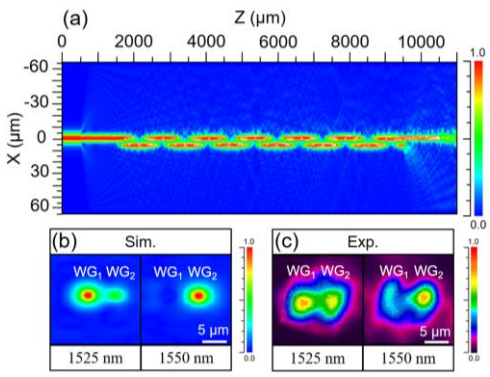

Fig. 4. (a) Simulated optical field distribution within the fiber directional coupler. Mode profiles output at different wavelengths (b) simulated results; (c) measured results.

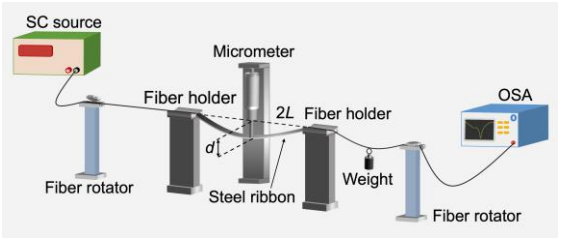

Fig. 5. Experimental setup for bending measurement.

Fig. 5 illustrates the experimental setup for vector bend measurement. The fiber directional coupler was placed in the middle of two fiber holders and the SMF pigtails of the fiber directional coupler were held in place using two fiber rotators. The fiber directional coupler was covered with a steel ribbon so that the bending can be evenly distributed across the fiber structure. A 2-g weight was used to make sure the fiber was taut and thus that the fiber and the steel ribbon remain in contact during the bending process. By adjusting the micrometer, the descending spindle will change the curvature of the steel ribbon and that of the fiber directional coupler. The bending curvature can be calculated as $C=2d/(d^2+L^2)$, where d is the displacement of the spindle, and L is half the distance between the two fiber holders. After each bend measurement, the fiber rotators on the left and right sides are rotated by a determined angle, to carry out vector bend measurement.

The bending response characteristics of the fiber directional coupler structure in the range of 0° to 180° were measured. Fig. 6(a)-(c) show the transmission spectrum evolution results for three selected bending orientations of 0°, 90° and 180°. It is found that the spectrum exhibits a blue-shift when the curvature increases at 0° and 90°, while there is a red-shift at 180°. This can be explained by the asymmetric distribution of the two waveguides in the NCF. When the fiber is bent in different directions, the effective RI of the mode in WG_2 increases or decreases depending on whether it is stretched or compressed, while the effective RI of the mode in the central WG_1 is almost invariant, resulting in a bending-dependent spectral shift response. Furthermore, within the same curvature change range of 0 to 0.62 m^{-1}, the spectral shift magnitude is different. The dip A and B wavelength shifts as a function of curvature change for all bending orientations were linearly fitted and are shown in Fig. 6(d) and Fig. 6(e), respectively. It can be observed that the fiber directional coupler shows good linear response to curvature changes. The bending sensitivities of dip A were determined to be -87.23 nm/m^{-1}, -46.39 nm/m^{-1}, -13.45 nm/m^{-1}, 33.25 nm/m^{-1} and 78.29 nm/m^{-1} for the bending orientations of 0°, 45°, 90°, 135° and 180°, respectively, and the bending sensitivities of dip B were determined to be -97.11 nm/m^{-1}, -31.50 nm/m^{-1}, -11.42 nm/m^{-1}, 29.38 nm/m^{-1} and 58.22 nm/m^{-1} for the bending orientations of 0°, 45°, 90°, 135° and 180°, respectively.

In order to determine the bending orientation, a wavelength-bending coordinate system was established with the wavelengths of dip A and dip B as the x-axis and y-axis. As shown in Fig. 7(a), the specific bending orientation information can be unambiguously determined based on a knowledge of λ_A and λ_B. The corresponding curvature is determined from the linear fitting results in Fig. 6. The above bending measurements confirm that the fiber directional coupler in this investigation has good vector bending measurement capability.

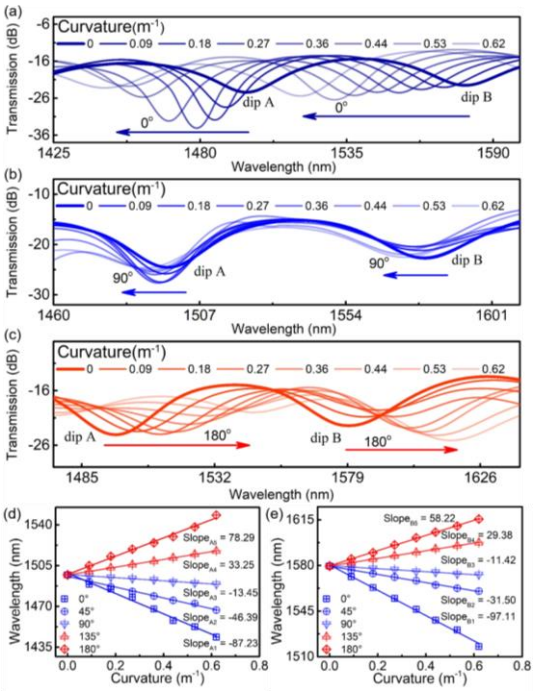

Fig. 6. Evolution of the transmission spectra of the fiber directional coupler when the curvature is changed at different orientations of (a) 0°; (b) 90°; (c) 180°. Wavelength shifts versus curvature variation for different orientations (d) dip A; (e) dip B.

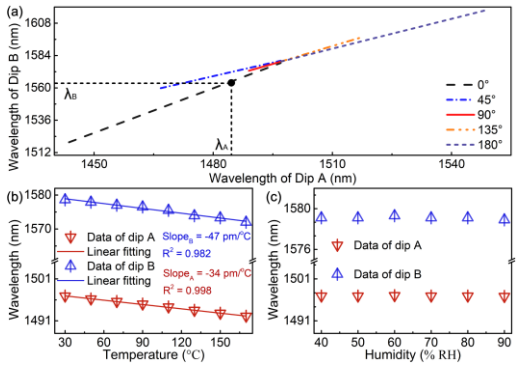

Fig. 7. (a) Resonance wavelengths of dip A and dip B against curvature. The response of the fiber directional coupler to (b) temperature; (c) humidity.

The temperature and humidity response characteristics of the fiber directional coupler were also investigated experimentally. In the temperature test, the temperature was increased from 30 °C to 170 °C with a step size of 20 °C. It can be seen from Fig. 7(b) that with increasing temperature, there is a blue-shift in the wavelength of dip A and dip B. The temperature sensitivities were determined to be -34 pm/°C for dip A and -47 pm/°C for dip B, respectively. Given the measured bending and temperature sensitivities, the maximum bend-temperature cross-sensitivity of the sensor is calculated to be 0.0041 m^{-1}/°C. In the humidity test, the humidity was increased from 40 %RH to 90 %RH with a step size of 10 %RH. It is noted that when the external humidity changes, no discernible wavelength shift can be observed, as evident in Fig. 7(c). This means that the fiber directional coupler is insensitive to humidity, thereby ensuring the accuracy and stability of vector bending measurement in environments where humidity changes are expected.

In summary, a fiber directional coupler was fabricated in an NCF using a fs laser and demonstrated as a sensor for vector bend measurement. Due to the asymmetry introduced by the written waveguides, the fiber directional coupler exhibits a good bending-dependent spectral shift response. In the 0° bending orientation, the maximum bending sensitivity is as high as -97.11 nm/m^{-1}. In addition, the immunity of the fiber directional coupler to ambient humidity changes was also confirmed. As a result of its high bend sensitivity and vector measurement capability, along with an immunity to changes in ambient humidity, the proposed fiber directional coupler could be a valuable tool for highly sensitive structural health monitoring for aerospace and deep-sea exploration equipment.

Funding. National Natural Science Foundation of China (NSFC) (62225502, 61935006, 62090062, 62205085); Heilongjiang Provincial Natural Science Foundation of China (LH2020F028); Fundamental Research Funds for the Central Universities (3072022TS2504); 111 Project (B13015); Heilongjiang Touyan Innovation Team Program; Science Foundation Ireland under the Centres research program for the MaREI project (SFI/12/RC/2302_P2).

Disclosures. The authors declare no conflicts of interest.

Data availability. No data were generated or analyzed in the presented research.

REFERENCES

1. C. Li, D. Liu, C. Xu, Z. Wang, S. Shu, Z. Sun, W. Tang and Z. Wang, Nat. Commun. **12**, 2950 (2021).
2. K. Tian, Y. Xin, W. Yang, T. Geng, J. Ren, Y. Fan, G. Farrell, E. Lewis, and P. Wang, J. Lightwave Technol. **35**, 1725 (2017).
3. M. Hou, K. Yang, J. He, X. Xu, S. Ju, K. Guo, and Y. Wang, Opt. Express **26**, 23770 (2018).
4. Y. Zhang, W. Zhang, L. Chen, Y. Zhang, S. Wang, L. Yu, Y. Li, P. Geng, T. Yan, X. Li, and L. Kong, Opt. Lett. **42**, 3892 (2017).
5. P. Chen, X. Shu, and K. Sugden, Opt. Lett. **43**, 531 (2018).
6. T. Liu, H. Zhang, B. Liu, X. Zhang, H. Liu, and C. Wang, IEEE Sens. J. **19**, 3343(2019).
7. W. Li and D. Wang, Opt. Lett. **43**, 3405 (2018).
8. S. Zhang, L. Yin, Y. Zhao, A. Zhou, and L. Yuan, Opt. Laser Technol. **120**, 105679 (2019).
9. R. Wang, K. Tian, M. Zhang, Z. Zhao, G. Farrell, E. Lewis, and P. Wang, J. Lightwave Technol. **40**, 6501 (2022).
10. J. Villatoro, V. P. Minkovich, and J. Zubia, Opt. Lett. **40**, 3113 (2015).
11. J. R. Guzman-Sepulveda, and D. A. May-Arrioja, Opt. Express **21**, 11853 (2013).
12. J. Yang, C. Guan, Z. Yu, M. Yang, J. Shi, P. Wang, J. Yang, and L. Yuan, Sens. Actuators B Chem. **305**, 127555 (2020).
13. D. J. J. Hu, P. P. Shum, J. L. Lim, Y. Cui, K. Milenko, Y. Wang, and T. Wolinski, IEEE Photon. J. **4**, 2010 (2012).
14. J. Han, Y. Zhang, C. Liao, Y. Jiang, Y. Wang, C. Lin, S. Liu, J. Wang, Z. Zhang, J. Zhou, and Y. Wang, Opt. Express **28**, 14263 (2020).
15. Y. Kong and X. Shu, J. Light. Technol. **39**, 2194 (2021).
16. Y. Zhang, C. Lin, C. Liao, K. Yang, Z. Li, and Y. Wang, Opt. Lett. **43**, 4421 (2018).
17. L. Bo, P. Wang, Y. Semenova, and G. Farrell, IEEE Photon. Technol. Lett. **25**, 228 (2013).
18. G. Yin, F. Zhang, B. Xu, J. He, and Y. Wang, Opt. Express **28**, 14850 (2020).